Journal of Materials Processing Tech. 252 (2018) 720–727

Contents lists available at ScienceDirect

Journal of Materials Processing Tech.

journal homepage: www.elsevier.com/locate/jmatprotec

Keyhole-induced porosity formation during laser welding

Jiajun Xu[a,b], Youmin Rong[a,b], Yu Huang[a], Pingjiang Wang[a,*], Chunming Wang[b]

[a] State Key Lab of Digital Manufacturing Equipment and Technology, School of Mechanical Science and Engineering, Huazhong University of Science and Technology, Wuhan, China

[b] School of Material Science and Engineering, Huazhong University of Science and Technology, Wuhan, China

ARTICLE INFO

Keywords:
Laser beam welding
Porosity formation
Bubble development
Keyhole dynamics
Molten pool dynamics

ABSTRACT

Through laser welding experiment with glass, the dynamics of keyhole and molten pool could be directly observed to reveal the mechanism of porosity formation using high speed camera. The high speed images showed that large fluctuation of keyhole was responsible for the increased bubble formation, and bubble merging resulted in the formation of large pore. The porosity of the welded samples was characterized qualitatively and quantitatively by combining super depth microscope and image processing. Porosity characteristics such as pore number, pore diameter (maximum and mean), porosity volume and porosity ratio varied with changes in welding speeds and laser powers. Increased energy density led to a decrease in the number but an increase in the other characteristics, indicating that the higher the energy density the more violent the bubble merging and giving rise to an increased possibility to form large pores.

1. Introduction

Laser beam welding, due to its high energy density, high welding speed and narrow heat affected zone, has been widely applied in automobile, shipbuilding, aerospace and energy. Porosity is one of the most common and undesirable defects, which heavily degrades the properties of laser welds such as strength and fatigue. To suppress the defect, extensive studies have been performed aimed at understanding the formation of porosity and finding its driving forces.

Lin et al. (2017) reported pores could be divided into two types, one was keyhole-induced porosity, the other was metallurgical factor-induced porosity. The metallurgical factor-induced pores are caused by low boiling point elements (H and N) in alloys or contaminations on the surfaces being welded. The porosity is largely induced by keyhole in 316L stainless steel welding and the metallurgical factor-induced type are not studied in this paper.

Both in-process detections and post-process inspections are conducted to investigate the extremely complex dynamics of keyhole and molten pool during welding, which are the main driving forces for porosity formation. The in-process detections are performed by high speed camera, x-ray transmission imaging system and spectrometer. Seto et al. (2000) found that porosity formation was resulting from keyhole instability using a high speed optical and X-ray transmission imaging system. The images displayed that bubbles were formed when the unstable keyhole collapsed and the dynamics of keyhole and plasma had a close relationship, suggesting that the plasma dynamics correlate with porosity formation. To overcome the problem that only the surface of samples can be observed when using high speed imaging, welding experiments with transparent materials such as glass, water and ice have been performed to observe the keyhole dynamics with low cost, high speed and high resolution. Berger et al. (2011) found that the keyhole as well as the bubble were partly filled with shielding gas and partly with metal vapor during the experiments with water and ice.

The post-process inspections are performed to define the relationship between porosity defect and welding parameters by means of metallographic sectional analysis, X-ray radiography and 3D X-ray tomography. Laser power and welding speed play a large role in porosity formation. Porosity ratio decreased with the increased welding speed according to Madison and Aagesen (2012), while increased with the increased laser power according to Yu et al. (2010). The characteristics of molten pool, which are dependent upon laser power and welding speed, correlate with porosity formation. Zhang et al. (2017) proposed a volume characteristic coefficient to predict porosity area ratio. Norris et al. (2011) indicated that the average pore size increased linearly with the area of weld cross-sectional during partial penetration laser welding with 304L stainless steel. As the main portion of porosity, shielding gas are strongly associated with porosity formation. Mazar Atabaki et al. (2015) reported that porosity ratio could be best mitigated by applying the side shielding gas of 92%Argon–8%CO in hybrid laser/arc welds of advanced high strength steel. Elmer (2015) found the porosity still existed in A36 and 304L weld when using Ar but very low or no porosity when using N_2.

* Corresponding author.
E-mail addresses: xujiajun0811@163.com (J. Xu), pjwang_hust@163.com (P. Wang).

http://dx.doi.org/10.1016/j.jmatprotec.2017.10.038
Received 19 July 2017; Received in revised form 11 October 2017; Accepted 24 October 2017
Available online 06 November 2017

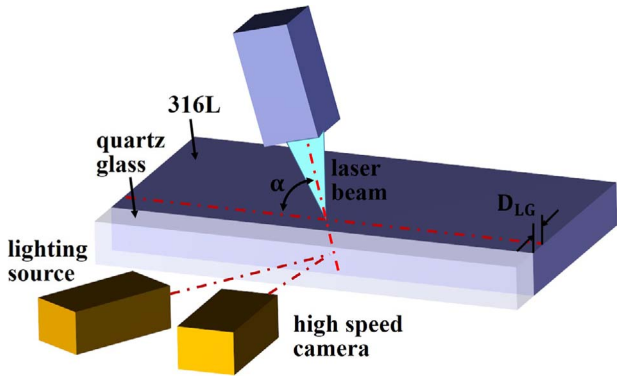

Fig. 1. Experiment setup schematic, where the angle between laser beam and work piece surface, ***α*** is 80°, and the distance of laser beam center to the edge of quartz glass, D_{LG} has two setups of 0.25 mm and 0.5 mm, respectively.

Table 1
Physical properties of the adopted materials in this study.

Material	Quartz glass	316L
Density, (kg m^{-3})	2200	7960
Thermal expansion coefficient, (K^{-1})	5.7×10^{-7}	1.893×10^{-5}
Thermal conductivity, (Wm^{-1} K^{-1})	1.4	14.15
Softening point, (°C)	1680	–
Melting point, (°C)	–	1375–1450

On the other hand, computational fluid dynamics (CFD) methods which can be considered as the combination of in-process detections and post-process inspections, have recently been applied not only to understand the keyhole dynamics and porosity formation mechanism, but also to give a more comprehensive guidance for welding parameter optimization to achieve a better quality weld. Lin et al. (2017) simulated porosity formation during laser welding, the results revealed that porosity formation experiences three steps: keyhole-induced bubble formation, bubble floating in the molten pool and pore formation with the solidifying molten pool. Panwisawas et al. (2017) developed a physics-based model to simulate keyhole and porosity formation, and summarized the effect of the welding parameters on maximum size of pore in a normalized processing diagram. However, the mechanism of porosity formation has not been fully investigated. Bubble development induced by molten pool dynamics, especially the development from a small to a large when bubble is floating in the molten pool, have rarely been studied.

In this paper, laser welding experiments with glasses were performed to directly observe the dynamics of molten pool and keyhole using high speed camera. Keyhole-induced bubble (KIB) formation and molten pool-induced bubble development were investigated aiming to reveal the mechanism of porosity formation.

2. Experimental procedure

The experiment setup is illustrated in Fig. 1. Laser welding experiments were conducted using a fiber laser (IPG YLS-4000) with a maximum output power of 4 kW, a wavelength of 1060 nm and a beam spot size of 0.35 mm in diameter. High speed imaging was performed on the quartz glass using a high speed camera (Phantom V611) together with a band-pass filter with a transmission band of 808 nm. A laser illuminating system (CAVITAR CAVILUX™ Smart) was employed to illuminate the welding zone, synchronizing with the high speed camera. This employs a pulse laser with a wavelength of 808 nm, an output power of 500W and a frequency ranging from 100 Hz to 100000 Hz. The images were taken at 2000 frames/s. The materials were 316L austenitic stainless steel in the dimension of 100 × 50 × 10 mm, and heat resistant quartz glass in the dimension of 100 × 5 × 20 mm. The target chemical compositions in weight percentage and physical properties of the stainless steel and glass are shown in Tables 1 and 2. The laser beam was focused on the stainless steel with a distance (D_{LG}) to the edge of quartz glass.

Table 3
Welding parameters adopted in the experimentation.

Welding parameters	Value
Laser power, (kW)	2.4, 2.7, 3.0
Welding speed, (m min^{-1})	1.0, 1.3, 1.6
Shielding gas flow, (m^3/h)	1.5
Defocusing distance, (mm)	−3
Distance between laser beam and glass (D_{LG}), (mm)	0.25, 0.5

Pang et al. (2016) reported that keyhole had a diameter of 0.33 mm at the neck and a maximum temperature of approximately 2800 °C on the wall during the laser beam welding simulation of stainless steel using 1500W laser power and 3 m/min welding speed. This indicates that molten pool behind keyhole cannot be observed because the glass is softened by the high temperature keyhole wall when the D_{LG} is too small, whereas keyhole cannot be observed when the D_{SG} is large enough to avoid glass softening due to the limited keyhole size. To directly observe the dynamic behaviors of weld pool and keyhole, two D_{LG}'s of 0.25 mm and 0.50 mm were employed. The welding parameters are shown in Table 3.

High speed images were processed to investigate keyhole dynamics using Matlab. The height of keyhole was considered as the characteristic parameter, the process is shown in Fig. 2. Otsu's method reported by N. Otsu (1979) was used to segment the images automatically. To improve the precision of threshold segmentation, a moving window was used to cut the images. A digital super depth microscope (KEYENCE VHX-1000C) was used to observe the microstructure and characterize the porosity of the 316L welds. Hough circle transform improved by Roushdy (2007) was carried out to detect the pores of the microstructure images in 50 magnifications. The transform was improved in this study, with which the diameter of every pore can be detected with high efficiency and high spatial resolution. The resolution can be as fine as 4.12 µm. Porosity characteristics such as pore number, pore diameter, porosity volume and porosity ratio in each laser welded weld were calculated.

3. Results and discussion

3.1. Bubble formation mechanism

Wang et al. (2012) reported that plasma during laser beam welding could be divided into keyhole plasma and floating plasma both with a fluctuation in size. Keyhole plasma, the size of which can be seen as the size of keyhole, is the main portion of plasma with the most brightness, whereas floating plasma is with little brightness above the surface of

Table 2
Chemical compositions of the adopted materials (wt-%).

Element	SiO_2	C	Si	Mn	P	S	Cr	Mo	Ni
316L	–	0.021	0.77	1.019	0.039	0.001	16.92	2.03	12.16
Glass	99.97–99.99	–	–	–	–	–	–	–	–